ACS SENSORS

pubs.acs.org/acssensors

Article

Imaging of CO_2 and Dissolved Inorganic Carbon via Electrochemical Acidification–Optode Tandem

Alexander Wiorek, Fabian Steininger, Gaston A. Crespo, Maria Cuartero,* and Klaus Koren*

Cite This: *ACS Sens.* 2023, 8, 2843–2851

Read Online

ACCESS | Metrics & More | Article Recommendations | Supporting Information

ABSTRACT: Dissolved inorganic carbon (DIC) is a key component of the global carbon cycle and plays a critical role in ocean acidification and proliferation of phototrophs. Its quantification at a high spatial resolution is essential for understanding various biogeochemical processes. We present an analytical method for 2D chemical imaging of DIC by combining a conventional CO_2 optode with localized electrochemical acidification from a polyaniline (PANI)-coated stainless-steel mesh electrode. Initially, the optode response is governed by local concentrations of free CO_2 in the sample, corresponding to the established carbonate equilibrium at the (unmodified) sample pH. Upon applying a mild potential-based polarization to the PANI mesh, protons are released into the sample, shifting the carbonate equilibrium toward CO_2 conversion (>99%), which corresponds to the sample DIC. It is herein demonstrated that the CO_2 optode–PANI tandem enables the mapping of free CO_2 (before PANI activation) and DIC (after PANI activation) in complex samples, providing high 2D spatial resolution (approx. 400 μm). The significance of this method was proven by inspecting the carbonate chemistry of complex environmental systems, including the freshwater plant *Vallisneria spiralis* and lime-amended waterlogged soil. This work is expected to pave the way for new analytical strategies that combine chemical imaging with electrochemical actuators, aiming to enhance classical sensing approaches via in situ (and reagentless) sample treatment. Such tools may provide a better understanding of environmentally relevant pH-dependent analytes related to the carbon, nitrogen, and sulfur cycles.

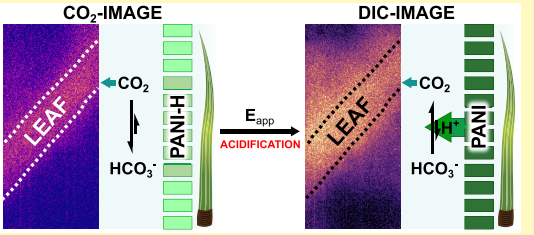

KEYWORDS: *optode, polyaniline, electrochemical acidification, plant respiration, soil, spatial resolution, carbonate chemistry, carbonate alkalinity*

Dissolved inorganic carbon (DIC) is defined as the sum of inorganic carbon species in water and plays a major role in many biological and environmental systems. Measurement of DIC is important to gain a fundamental understanding of the carbonate chemistry and to comprehend fluxes in the global carbon cycle.[1] In aquatic ecosystems, DIC acts as a primary source of carbon for photosynthesis and has a function in controlling the pH.[2,3] Importantly, increasing anthropogenic CO_2 gas emissions are leading to continuous ocean acidification, which can pose a significant threat to marine life, including calcifying organisms like corals, mollusks, and some phytoplankton species.[4,5] Accordingly, the accurate assessment of DIC in water is essential to preserve the integrity of aquatic ecosystems and marine ecology, in particular.

Conventional methods to measure DIC in water are based on multiple-step, laboratory-based techniques involving the conversion of inorganic carbonates to CO_2 by acid treatment, followed by coulometric titration or infrared spectroscopy analysis.[6,7] While these methods allow for high-precision measurements,[8] careful water sampling to avoid exchange with atmospheric CO_2 and the addition of several reagents to the sample are required. Additionally, spatial resolution is limited in these sampling-based approaches, making them unsuitable to investigate chemical microenvironments often found in complex samples (e.g., individual corals,[9] plants,[10] or soils[11]). As a result, other techniques have been introduced over the years to investigate the carbonate system at a higher spatial resolution. In such a context, potentiometric probes have been used to characterize the water column (meter resolution),[12] while amperometric microsensors were utilized to measure at a small scale, close to seagrass leaves (<mm).[13] In both cases, the calculation of DIC relied on the simultaneous measurement of pH and one carbonate species (CO_2 or CO_3^{2-}). However, these calculations are often not accurate enough, as they require precise determination/knowledge of all the equilibrium constants in the carbonate system,[14] and the intrinsic errors of each sensor (e.g., noise, drift, etc.) may also influence the final result in an accumulative way.

Received: April 23, 2023
Accepted: June 6, 2023
Published: July 1, 2023

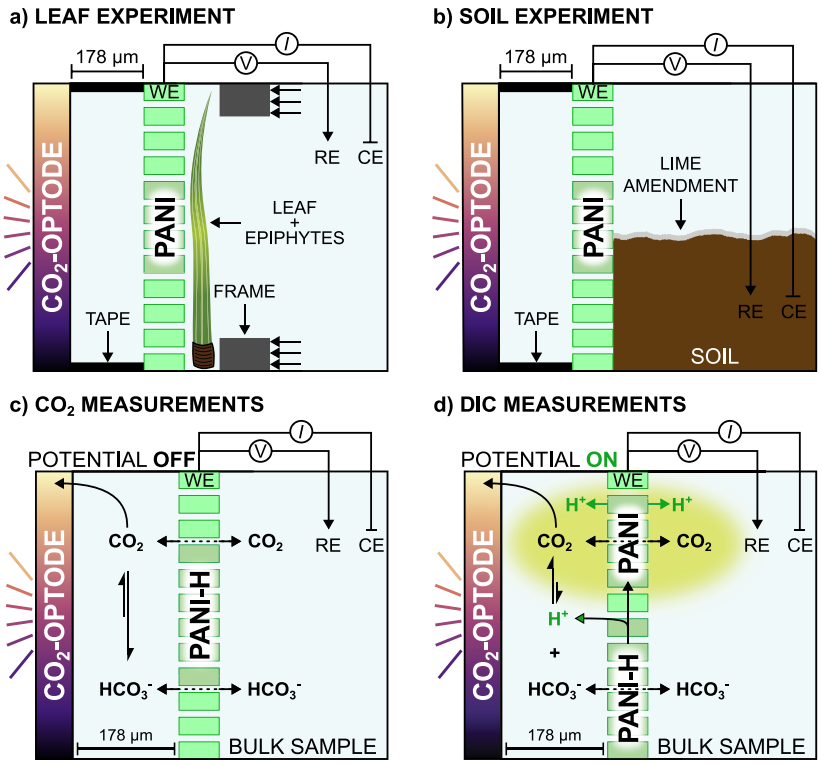

Figure 1. Top part: experimental setups for CO_2 and DIC measurements in real samples. (a) Freshwater leaf. (b) Soil. Bottom part: mechanism underlying the PANI−optode tandem measurements. (c) CO_2 measurements before PANI-based acidification. CO_2 diffuses from the bulk sample through the PANI mesh toward the CO_2 optode, where it is quantified. (b) DIC measurements after PANI-based acidification. DIC diffuses from the bulk sample into the tiny sample space, where it is converted to measurable CO_2. In the electrochemical cell PANI acts as the WE, the RE is an Ag/AgCl wire, and the CE is a Pt rod.

A recent work proposed the implementation of an outer acidic conversion chamber with an amperometric CO_2 microsensor.[15] Passive diffusion-based acidification generated the in situ conversion of inorganic carbonates to measurable CO_2. Additionally, various electrochemically driven acidification procedures have been proposed in combination with sensors to measure certain parameters of the carbonate system. For example, electrochemical water splitting[16] and permselective membranes[17] permit the modification of pH close to optical and potentiometric pH sensors to measure alkalinity. Polyaniline (PANI) has been shown to release a significant number of protons upon its oxidation to acidify environmental samples.[18] This phenomenon was specifically used for the detection of alkalinity[19] and dissolved inorganic phosphorus.[20] Moreover, in a recent letter, the combination of a PANI mesh electrode with a planar pH optode has allowed for the 2D visualization of PANI-mediated electrochemical acidification in diverse samples. The concept was also used to map buffer capacity gradients in heterogeneous samples.[21] Effectively, a PANI mesh can homogeneously shift the pH below 4.5 in samples at environmental buffer concentrations (<10 mM bicarbonate equivalents), which corresponds to 99.9% conversion of all the dissolved inorganic carbonate species to CO_2.[22]

In this work, we demonstrate the use of a PANI mesh electrode to locally acidify a sample in contact with a planar CO_2 optode−PANI architecture, which allows DIC to be characterized with high spatial resolution. First, a thorough characterization of the PANI−optode tandem was accomplished in artificial samples, providing evidence that the system operates under diffusion-limited control. Then, the PANI−optode tandem was used to analyze various environmental samples, obtaining unique information about their carbonate chemistry. This includes the DIC mapping during a dark respiration event of a freshwater leaf (*Vallisneria spiralis*) covered with an epiphytic biofilm and the characterization of waterlogged soil samples.

EXPERIMENTAL SECTION

Experiments with the PANI−optode tandem were performed in a small glass aquarium (350 mL, see Figure S1a,b), which was filled with the respective solution/sample and where the reference (RE) and counter electrodes (CE) were positioned. The CO_2 optode was taped inside the aquarium using isolation tape (Scotch Super 33 + vinyl electrical tape) before pressing the PANI mesh onto the optode. The PANI mesh synthesis was based on a previously published protocol (see Figure S2).[19,21] For sample acidification, the PANI mesh was activated by applying a constant potential of 0.4 V with respect to the open circuit potential (OCP) for 600 s. This process was previously demonstrated to decrease the sample pH to levels of <4.5.[21] For more information about the PANI synthesis, experimental setup, equipment, chemicals, and calibration protocol, the reader is referred to the Supporting Information.

For the real sample analysis, a leaf of the freshwater plant *Vallisneria spiralis* covered with an epiphytic biofilm was cut, pressed onto the PANI−optode tandem, and submerged into the aquarium, as illustrated in Figure 1a (see Figure S1c for real images). Stirring and illumination were activated for 30 min to ensure fully oxic conditions. Then, the stirring was stopped, and the sample was incubated in dark conditions for 1 h. Afterward, the PANI-based acidification was performed, and pictures were acquired in 30 s intervals over a period of 15 min.

Sandy loam soil was collected from 0 to 20 cm depth in Foulum, Denmark (56.4983, 9.5657), sieved (4 mm mesh diameter), and

https://doi.org/10.1021/acssensors.3c00790
ACS Sens. 2023, 8, 2843−2851

stored at 4 °C prior to the experiment. The soil had a relatively low initial pH of 5.6. The soil packing procedure was adopted from Zhu et al.[23] and Nguyen et al.[24] The the measurement chamber in the aquarium was packed with 120 g of soil (final thickness of 4 cm), resulting in a bulk density of 1.3 g/cm^3. The PANI−optode tandem was then pressed firmly against the soil before closing the chamber, as illustrated in Figure 1b (see Figure S1d for real pictures). The top part of the soil was amended with 4 g/kg calcium carbonate,[25] and a rain event was simulated by the addition of 31 mL of water over a period of 180 min (corresponding to a 17 mm h^{-1} rain event), resulting in fully waterlogged soil. After that, the PANI-based acidification was carried out, and pictures were acquired in 30 s intervals over a period of 15 min.

RESULTS AND DISCUSSION

We present an actuator-sensor principle for the chemical imaging of pH-dependent species, using an electrochemical actuator (i.e., PANI) for pH modulation to values lower than pH 4.5 that is placed in proximity to a planar optode. Notably, the optode is selective for only one of the species involved in the pH-dependent equilibrium. In this paper, we have selected the carbonate system (CO_2 optode) as the proof-of-concept. It is expected that the speciation of the analyte changes according to an induced pH shift in the sample (i.e., conversion of CO_3^{2-}/HCO_3^- to CO_2), which will ultimately result in a change of the optode signal. As illustrated in Figure 1, we have developed an analytical concept to obtain chemical images of both CO_2 before the PANI activation (Figure 1c) and DIC after the acidification of the sample (Figure 1d).

To obtain an actuator capable of modulating a decrease in pH in 2D, PANI was electrodeposited on a rigid stainless-steel mesh (36% of open area and 150 μm thickness after the PANI deposition). For the proton release, the PANI mesh acts as the working electrode (WE) in a three-electrode cell, together with the reference electrode (RE) and counter electrode (CE) located in the sample bulk. The CO_2 optode was taped onto one of the walls of the glass aquarium, and the PANI mesh was put close to the optode by clamping it with a plastic frame (Figure S1a,b). A tiny layer space is created between the optode and the mesh (thickness of ∼178 μm, equal to the thickness of the tape). The final area achieved for measurements was approximately 2 × 5 cm. In principle, larger areas could be reached by using a larger PANI mesh and a larger optode. This will require an additional spacer to maintain a homogeneous thickness in the tiny sample layer throughout the whole area. Because of the open area of the mesh, the sample will locally equilibrate between the tiny layer space and the bulk sample. Therefore, the imaging will provide information directly related to the sample.

Initially, the readout of the optode corresponds to the concentration of free CO_2 dissolved in the solution, which is dictated by the initial sample pH and the natural carbonate equilibrium (Figure 1c). Then, a localized acidification down to pH < 4.5 is activated by the electrochemical oxidation of PANI (0.4 V versus the OCP for 600 s) from its leucoemeraldine (reduced from) into emeraldine (partially oxidized form) structures with a concomitant release of protons.[18] The established pH decrease shifts the carbonate equilibrium and generates dissolved CO_2, which is detected by the optode (Figure 1d). Importantly, if the pH is decreased down to 4.5 or lower, the final optical readout will correspond to approximately 99% of the total concentration of all dissolved inorganic carbonate species (see Figure S3 in the Supporting Information), thus representing the DIC of the sample.[22]

Overall, we expect the PANI−optode tandem to be able to quantify free CO_2 (before PANI activation) and DIC (after PANI activation) in a sample with adequate 2D resolution. To achieve this concept, the following operational aspects are to be considered. The PANI−optode tandem needs to be calibrated only once for each optode batch (i.e., at the beginning of its utilization). The PANI film is activated once per sample imaging, and then, it is regenerated before being used for the next sample (10 mM H_2SO_4 at 0 V versus the Ag/AgCl RE,[21] Supporting Information). With this regeneration procedure, the PANI mesh can be re-used for more than 70 activations over a minimum of two weeks.[19,20] Because of the regeneration step, the principle is not suitable for continuous but for discrete dynamic and/or long-term measurements of DIC along the lifetime of the PANI−optode system.

The actuator-sensor principle will primarily work on the basis of kinetic control (conversion of bicarbonate to CO_2 through carbonic acid)[26] and diffusion in the aqueous phase. Also, diffusion will dominate in the optode element (i.e., in the outer gas-permeable layer). Particularly, for the aqueous phase, (i) concentration gradients of protons and bicarbonate (opposite directions) across the tiny layer space, (ii) conversion of bicarbonate/carbonate to CO_2, and (iii) diffusion of CO_2 across the tiny layer space to the optode will occur. The total time expected for all these diffusion events was estimated to be ca. 100 s (Supporting Information, Section 2, and Table S1). Considering now the optode, (iv) diffusion across the gas permeable ion-exclusion outer membrane and (v) acid−base equilibria of the fluorescent indicator in the optical sensing layer are to be considered.

The PANI−optode tandem was first tested in a 3 mM bicarbonate solution (0.1 M NaCl background). Figure 2 shows the false color images (i.e., the ratio between the red and green channels of the camera, R/G) observed at selected times before, during, and after the PANI-based acidification. During the first minute, no change in the ratiometric readout was observed. After 2 min, once >90% of the total amount of protons had been delivered to the solution[21] (and thus, most of the bicarbonate in the sample layer is expected to have been converted into CO_2), the optode started to respond. A gradual increase in the ratio was observed until 9 min elapsed. After that, a homogeneous image, coinciding with the finalization of the acidification process (10 min), was reached. A steady state was found to be maintained even 2 min after the acidification was stopped (12 min image). Overall, it took 9 min for the system to provide a homogeneous image of the CO_2 in the sample.

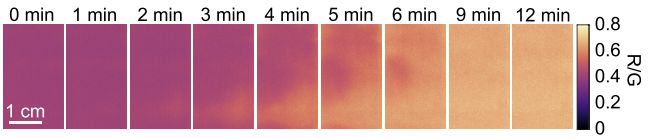

Figure 2. False color images provided by the CO_2 optode before, during, and after the PANI-based acidification was performed in a 3 mM bicarbonate solution. The activation of the PANI mesh was carried out at an applied potential of 0.4 V with respect to the OCP for 600 s.

Attempting to understand the response time of the PANI−optode system, we carried out a control experiment without the PANI mesh, minimizing the effect of any diffusion event (except that in the outer layer of the optode) under vigorous

https://doi.org/10.1021/acssensors.3c00790
ACS Sens. 2023, 8, 2843−2851

stirring conditions. To empirically estimate the response time intrinsic to the optode, we performed manual acidification and alkalinization of a bicarbonate solution while dynamically monitoring the response of the optode (Figure S4 in the Supporting Information). The observed response time was significantly shorter than that in the PANI−optode system: t_{95} = 147 ± 21 s (n = 3) compared to the 9 min observed in Figure 2. This indicated that the majority (70%) of the time needed to reach a homogeneous image is due to kinetic and diffusion events in the aqueous phase, as described above.

The response of the PANI−optode system was further investigated at increasing bicarbonate concentrations, from 1 to 5 mM. The dynamic responses of the CO_2 optode before, during, and after the corresponding PANI-based acidification are presented in Figure 3. Notably, a circular ROI with a

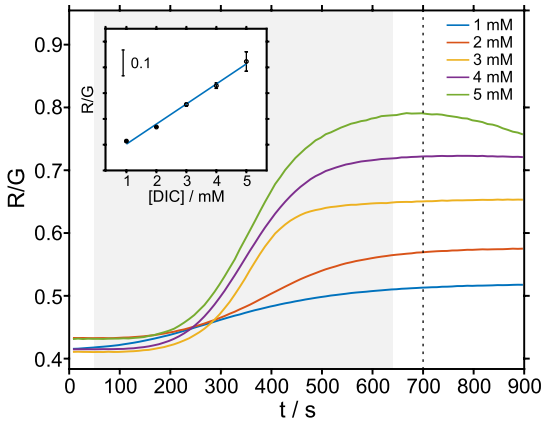

Figure 3. Dynamic response of the CO_2 optode during the PANI-based acidification (0.4 V versus the OCP for 600 s, gray area) observed for increasing bicarbonate concentrations in a 0.1 M NaCl background. The dashed line represents the time for the readout used to generate the calibration graph (60 s after the polarization potential for 600 s). Inset: calibration graph averaged from three measurements.

diameter of ca. 2 cm placed in the center of the optode was considered to average the R/G ratio. The response from triplicate measurements is presented in Figure S5.

For concentrations in the 1−3 mM range, the optode reached a steady signal after 450 s from the activation of the applied potential. The response time slightly increased for 4 and 5 mM concentrations (~650 s for 5 mM). This is likely because longer times are required to protonate increasing bicarbonate concentrations,[19] delaying the subsequent mass transport to the CO_2 optode. For the highest concentration (5 mM), the signal was found to slowly decrease from 700 s, probably due to the diffusion of bicarbonate from the bulk solution to the tiny space through the PANI-mesh, resulting in a neutralization of pH in the tiny layer space. For the rest of the concentrations, the signals were stable for at least 4 min from the time that the PANI activation was stopped. As a general trend, the optode signal was quite reproducible in the steady-state region, while larger variations were observed before the PANI activation and in the initial minutes of this process (Figure S5). This can be attributed to slight variations in the placement of the PANI−optode architecture in the system after removing/inserting the PANI mesh from/into the aquarium for its regeneration between the experiments. Advantageously, this is not expected to affect the calibration graph, which is obtained from the steady readouts, as explained below.

To establish a calibration curve for DIC (i.e., after sample acidification), the R/G value observed for each bicarbonate concentration at 60 s after the end of the electrochemical pulse was selected from the dynamic curves (dashed line in Figure 3). This timepoint represents a compromise between the time at which all inorganic carbonate species were successfully converted to CO_2 and avoiding the downward drift after the end of the pulse at the higher concentration of bicarbonate. The bicarbonate concentration in each standard solution is assumed to be equal to the DIC, which is only detected to its full extent by the CO_2 optode once the pH is reduced to pH 4.5 or lower. Importantly, the obtained calibration curve (inset in Figure 3) presented good linearity within the tested range (sensitivity = 0.078 mM^{-1} in the DIC range of 1−5 mM, R^2 = 0.993) and covered the expected DIC in most environmental samples.[3] The standard deviation was higher for the 5 mM concentration, coinciding with the lower fluorescence emission of the sensing layer.

The possible influence of the PANI mesh on the optode readout because of either electrochromism or an effect of the applied potential on the sensing layer was investigated by performing DIC calibrations using either the PANI's reduced (basal) or oxidized forms (Figure S6). Calibrations were performed at pH 3.7 (0.1 M citrate buffer), which results in a DIC to CO_2 conversion rate close to 100%.[27] We found a slight difference (i.e., a decrease) in the ratiometric signal when the PANI was in the oxidized form compared to the reduced one. The calibration using the reduced form of PANI (without any applied potential) presented a sensitivity of 0.106 mM^{-1} DIC (in the DIC range of 1−5 mM); in contrast, with the oxidized form of PANI (i.e., applying a potential of 0.4 V vs the OCP during the entire calibration), the sensitivity was slightly lower (0.090 mM^{-1} DIC, in the DIC range of 1−5 mM DIC). This could be explained by PANI presenting differences in electrochromism depending on the (initial) pH of the solution.[18] Nevertheless, the found difference was not substantial. However, the sensitivity when using the oxidized PANI was found to be higher (ca. 15%) than that observed in Figure 3. Additionally, there could be a slight influence of the applied potential in the optode response. In any case, it is advisable to perform the calibration as in Figure 3 (i.e., using the entire system with all the elements present) to account for the effects of the mesh, no matter their origin.

Next, the accuracy of the PANI−optode concept to quantify DIC was investigated by analyzing two real samples (n = 3): bottled mineral water (salinity = 0.12‰) and brackish seawater (salinity = 18.4‰). The samples were additionally characterized by means of conventional acid−base titrations (see Section 3 in the Supporting Information for the calculations). The samples were measured following the same procedure as that for the calibration graph: PANI-based acidification was conducted at a potential of 0.4 V versus the OCP for 600 s, and the final DIC value was determined from the response of the optode at 60 s after the acidification pulse was finished. The results are presented in Table 1. Notably, the acid−base titration of the seawater sample could overestimate the DIC concentration, as buffering species other than carbonates may be present in the sample (e.g., boric acid, silicates, or phosphates).[28] Nevertheless, the results obtained by the two methods presented a rather good agreement, with differences of <8%. Furthermore, the outcomes demonstrated

https://doi.org/10.1021/acssensors.3c00790
ACS Sens. 2023, 8, 2843−2851

Table 1. DIC Detection in Real Water Samples

sample	DIC (mM)			difference (%)
	PANI−optode	titration	references	
mineral water	2.07 ± 0.08	2.23 ± 0.03	2.3[a]	7.2
seawater	1.68 ± 0.09	1.82 ± 0.00	1.8−1.9[29]	7.7

[a]Manufacturer's label.

the versatility of the PANI−optode concept to be used in both freshwater and seawater samples.

The capability of the PANI−optode tandem for determining DIC in a heterogeneous system was further studied. For this purpose, an artificial chemical gradient was generated in a bicarbonate sample. As illustrated in Figure 4a, a plastic tube

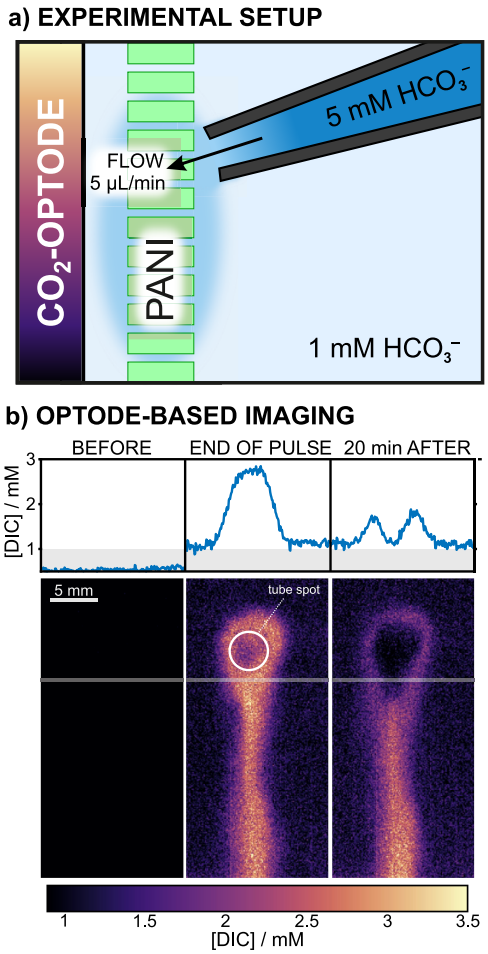

Figure 4. (a) Schematics of the experimental setup to create an artificial DIC gradient in the sample. (b) False-color images of DIC concentrations before and after the acidification pulse (just at the end and 20 min later). The gray lines in the pictures represent the analyzed line profile. The gray shaded areas in the graphs represent values which are below the calibration range.

with an inner diameter of approximately 3 mm and filled with 5 mM bicarbonate solution (in 0.1 M NaCl background) was placed close to the PANI−optode tandem, constantly introducing a higher bicarbonate concentration to the 1 mM bicarbonate (0.1 M NaCl) in the bulk solution placed in the aquarium. A flow rate of 5 μL/min achieved with a syringe pump was used to ensure a constant increased local bicarbonate concentration over time. The results of the DIC analysis before the acidification, just at the end of the pulse and 20 min after the acidification are shown in Figure 4b. Before applying the pulse, no response of the optode was observed.

Later, the PANI-based acidification resulted in increased CO_2 levels (i.e., corresponding to the total DIC) in the area where the more concentrated bicarbonate solution was introduced. Additionally, the injection angle (~30° downward) resulted in a downward flow of bicarbonate that generated a concentration gradient localized in a straight line from the tip outlet to the bulk sample. Notably, the measured DIC was not as high as the concentration of the introduced bicarbonate solution because of the immediate dilution upon contact with the sample in the aquarium. Finally, 20 min after stopping the acidification process and keeping the bicarbonate injection rate constant, it was observed how the local acidification effect gradually disappeared, i.e., an apparently lower DIC concentration was measured.

The outcomes in Figure 4b may provide an indication of the spatial resolution of the PANI−optode system by considering the spot of lower DIC in the images corresponding to the plastic tube of 3 mm diameter, which is labeled as the "tube spot" for clarification. In general, the imaging resolution of a planar optode is limited by the camera resolution (μm resolved per pixel) and the thickness of the sensing layer (i.e., diffusivity of the analyte within it), which governs how well a point source or gradient can be resolved.[30] However, this is not the limiting factor in the PANI−optode system, as the following rationalizes.

The aqueous layer confined between the mesh and optode could be assumed as a part of the sensing layer. Thus, a thicker layer will contribute to a longer diffusion pathway, resulting in an increase of diffusive smearing in the obtained picture.[31] The total distance between the sample (i.e., at the sample−mesh interface) and the point of readout (in the sensing layer) is estimated to be 300−400 μm, summing up the individual parts of the system (mesh, tiny sample space, and optode). The camera provides a resolution of approximately 70 μm per pixel, and hence, it is not expected to be the limiting factor for imaging resolution. Examining now the tube spot in Figure 4b more in detail, it displays a radius of ca. 1.9 mm, which is 0.4 mm larger than the tube size, thus confirming the expected diffusional-related smearing and a sub-mm resolution of the system.

With the confirmed ability to map DIC gradients in 2D, more complex heterogeneous samples were investigated and discussed in the following paragraphs. A leaf of the freshwater plant *V. spiralis* was put in contact with the mesh part of the PANI−optode tandem (Figure 5a), introduced in the aquarium setup, and incubated in freshwater (0.42‰ salinity) in dark conditions for 1 h before the acidification experiment was initiated (Figure 1a). Notably, the leaf was covered with a thick epiphyte layer consisting of phototrophic and heterotrophic microorganisms. This epiphyte layer can lead to strong basification, thereby reducing CO_2 and bicarbonate availability for photosynthesis in light conditions and increasing CO_2 concentrations and hypoxia at the leaf surface in dark conditions.[13] Images obtained before PANI-based acidification (Figure 5b) revealed how CO_2 levels evolved around the leaf from respiration in the dark (up to 0.9 mM in the center of the leaf), indicating increased levels of DIC. Increasing CO_2 concentrations likely caused a localized drop in pH around the leaf. Epiphytes were more abundant in the top part of the

https://doi.org/10.1021/acssensors.3c00790
ACS Sens. 2023, 8, 2843−2851

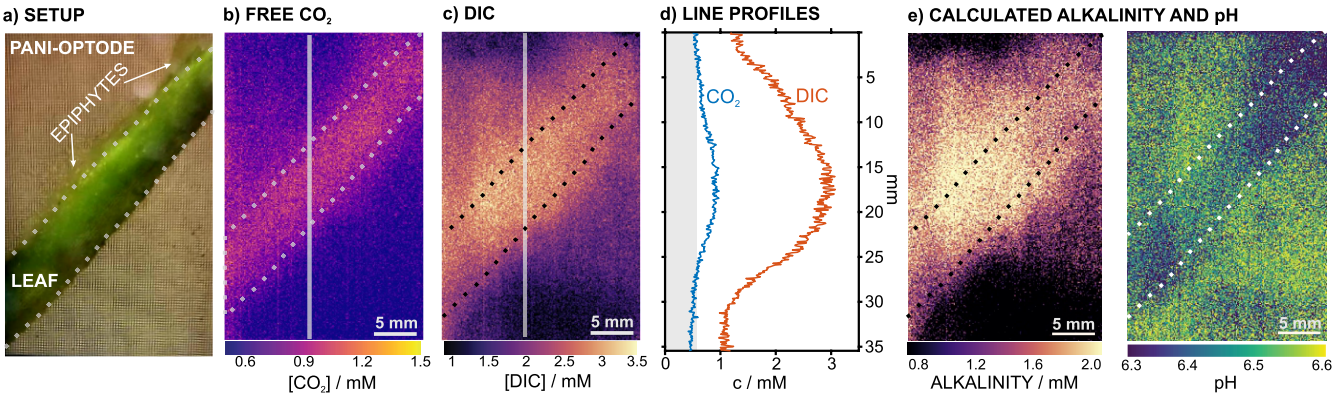

Figure 5. Imaging of an epiphyte-covered leaf of the freshwater plant *V. spiralis* during dark respiration. (a) Setup of the leaf on top of the PANI−optode architecture. (b) Image of free CO_2 after 1 h of incubation in freshwater under dark conditions. (c) Image of DIC right after PANI-based acidification. (d) Line profiles for CO_2 and DIC associated with the gray lines traced in (b,c) from the top to the bottom area. The gray area represents values below the CO_2 optode calibration range. (e) Calculated images for carbonate alkalinity and pH.

leaf, which resulted in localized differences (i.e., increases) in CO_2 in the surroundings above the leaf. In contrast, areas below the leaf with reduced microbial activity showed CO_2 concentrations below the limit of detection of the optode (0.5 mM).

Right after the PANI-based acidification (in dark conditions), once all carbonate species were converted to CO_2, the DIC concentrations around the leaf were visualized (Figure 5c). While higher levels were observed around the center of the leaf (up to 3 mM), there were also elevated concentrations of DIC present at short distances from the leaf. This becomes even more evident when inspecting the line profiles presented in Figure 5d, obtained from the gray lines highlighted in Figure 5b,c. The area around the leaf presents both the highest CO_2 and DIC concentrations (15−25 mm in the line profiles). Interestingly, areas of high epiphyte abundance (5−15 mm above the leaf) also showed increased DIC concentrations.

This trend was the same but less pronounced for free CO_2 concentrations (Figure 5b). The region in the line profile from 5 to 15 mm corresponded to zones with lower biological activity than that of the leaf, where the diffusion of DIC toward the solution became more pronounced. Notably, some deviations may be obtained for the CO_2 and DIC spatial distribution in the images because of the time elapsed between the two images (11 min), resulting in mass transport of DIC from the leaf (in the PANI−optode area) to the bulk solution.

The information on CO_2 and DIC collected with the camera for each pixel allowed for further calculations attempting to better describe the carbonate system in the leaf sample. In principle, any combination of two of the parameters involved in the overall carbonate system (i.e., DIC, CO_2, alkalinity, or pH) can be used to fully describe it.[2] Thus, the CO_2 and DIC measured from the chemical imaging approach were used to determine other parameters related to the carbonate system, such as pH and carbonate alkalinity, using eqs 1−4

$$K_1 = \frac{10^{-pH}[HCO_3^-]}{[CO_2]} \quad (1)$$

$$K_2 = \frac{10^{-pH}[CO_3^{2-}]}{[HCO_3^-]} \quad (2)$$

$$[DIC] = [CO_2]_{aq} + [HCO_3^-] + [CO_3^{2-}] \quad (3)$$

$$[Alkalinity] = [DIC] - [CO_2]_{aq} \quad (4)$$

where K_1 and K_2 are the equilibrium constants at a given salinity and temperature for the carbonate equilibria $HCO_3^- + H^+ \rightleftharpoons H_2O + CO_2$ and $HCO_3^- \rightleftharpoons H^+ + CO_3^{2-}$, respectively. These constants were calculated according to Roy et al.[14] Then, in the PANI−optode system, all the concentrations included in eqs 1−4 refer to the initial state prior to PANI-based acidification except for [DIC], which is in turn the final value read by the optode.

The estimation of alkalinity constitutes a straightforward calculation: the difference between DIC and free CO_2, according to eq 4. Evidently, the accuracy of the outcomes depends on that of the CO_2 and DIC measurements, and the combined errors of the two readouts must be considered.[32] Moreover, the estimation of pH can be performed at known salinity and temperature (herein 20 °C) using eqs 1−3. For acidic-neutral samples (pH ≤ 7) the contribution of carbonate to DIC becomes negligible, simplifying eq 3 into eq 5

$$[DIC] = [CO_2]_{aq} + [HCO_3^-] \quad (5)$$

where [DIC] and $[CO_2]_{aq}$ have been experimentally acquired in our experiments. Finally, by combining eqs 5 and 1, the pH can be calculated. However, if samples with a higher pH are investigated, the contribution of carbonate cannot be neglected, and both equilibria (eqs 1 and 2) must be considered.

The possibility of calculating the 2D distribution of alkalinity and pH was first confirmed from CO_2 and DIC results obtained in a 3 mM bicarbonate solution (0.1 M NaCl as background electrolyte: 5.9‰ salinity), with the pH adjusted to 6.1 (pK_{a_1} estimated at the experimental conditions[14]). Notably, by setting the pH equal to the pK_a, approximately 50% of the DIC would be present in the sample as free CO_2 and 50% as bicarbonate, hence potentiating the initial CO_2 imaging (1.5 mM, i.e., 50% of the initial bicarbonate concentration). The experimental results before and after PANI-based acidification, together with the images calculated for alkalinity and pH, are shown in Figure S7 in the Supporting Information. Considering that the measured concentrations of free CO_2 and DIC presented the expected readouts (1.5 and 3 mM, respectively), we proceeded to calculate the alkalinity and pH in 2D using eqs 1 and 5 (Figure S7b). Effectively, a pH of 6.1 and carbonate alkalinity of 1.5 mM were calculated from

https://doi.org/10.1021/acssensors.3c00790
ACS Sens. 2023, 8, 2843−2851

the measurements, which agreed with the experimentally controlled conditions.

Next, we utilized the same approach to calculate the distribution of carbonate alkalinity and pH around the freshwater plant leaf (Figure 5e). The calculated alkalinity map resembled the distribution of DIC in the sample, with higher concentrations around the leaf surface and gradually decreasing levels going further away from the leaf (areas where free CO_2 was below the limit of detection were excluded from the calculations and are not presented in the figure). In contrast, the pH showed a rather homogeneous distribution, with only slightly lower values at the location of the leaf and around the epiphytes. In this area, continuous CO_2 production during respiration under dark conditions is expected. Considering the overall low buffer capacities of many freshwater bodies, this localized CO_2 production can result in a slight decrease in pH. This effect is more pronounced in the areas of the PANI−optode that are covered by the leaf because this limits the mass transport of the bulk solution in the aquarium. Moreover, a lower pH can be observed in the top right corner of the pH map in Figure 5e, which is rich in epiphytes (see Figure 5a).

Finally, we used the PANI−optode analytical technology to investigate acidic soil samples. Importantly, soil acidity is a major problem in crop production and affects about 30% of the total ice-free area in the world.[33] Soil acidity can result in inhibition of plant growth due to nutrient deficiencies, have a negative impact on root hair length and growth[34] and lead to increased solubility of toxic metal ions such as aluminum.[35] To counteract these adverse effects, highly alkaline substances (e.g., gypsum or lime) are applied to the topsoil to mitigate some of these adverse effects by neutralizing the soil pH.[36] To mimic such an event, we packed acidic soil (pH 5.6, see Table S2) into a polymethyl methacrylate (PMMA) chamber and amended the topsoil with calcium carbonate ($CaCO_3$). After simulating a rain event of 17 mm h^{-1} by adding 31 mL of water for 180 min, the soil was fully waterlogged, and both CO_2 and DIC imaging measurements were conducted. Figure S8a in the Supporting Information depicts images of the soil treatment and the experimental setup. Notably, in the PANI−optode setup, DIC can only be measured in samples with sufficient water content, as the diffusion of ionic species into the tiny space between the PANI and optode must occur for the principle to work.

Figure 6a shows the resulting CO_2 and DIC concentration maps before and after PANI-based acidification respectively. While in some areas a minor increase in CO_2 (<0.8 mM) was observed, these levels are rather low compared to the DIC concentrations, which were found to be up to 2.2 mM. The DIC image indicated that there was a drastic increase in the soil pH because of the carbonate amendment (see Figure S8b for measurements without the $CaCO_3$ amendment). To assess the effectivity of the soil amendment, the pH can be obtained (according to eqs 1 and 5) from the CO_2 and DIC concentrations in the area where some initial CO_2 was detected. An increase in soil pH of approximately one unit was observed in the zone of 0−10 mm in the line profile (Figure 6b). However, the change was probably even higher in areas where no free CO_2 could be initially detected, i.e., above 12 mm in the line profile. Unfortunately, the pH calculations became inaccurate because the measured CO_2 was below the limit of detection (light green part of the pH spatial profile). Moreover, concentrations of free CO_2 and DIC were found to

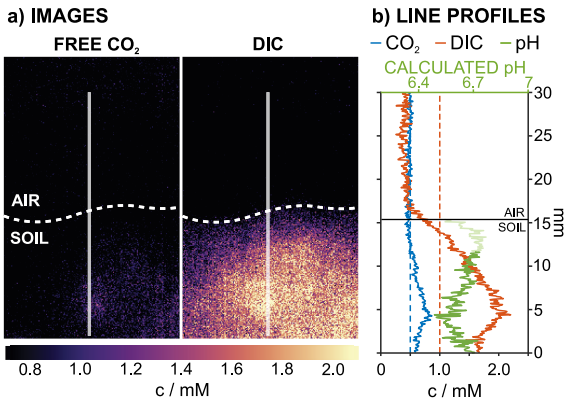

Figure 6. (a) False color images of free CO_2 and DIC concentrations in a carbonate-amended waterlogged soil sample. (b) Line profiles of CO_2, DIC, and pH corresponding to the gray lines traced in (a). The dashed lines represent the lower limit covered by the calibration of the optode for the respective analytes. The light green part of the pH profile represents calculated values where the measured CO_2 was below the limit of detection, thus making these pH values less accurate.

decrease close to the air−soil interface. We can find two possible explanations for this. First, because the surface of the soil was amended with $CaCO_3$, this could provide a local concentration of bicarbonate that is too high for the PANI to fully convert it to CO_2. Second, the generated CO_2 can equilibrate at the soil−air interface, providing an apparent gradient found between 10 and 15 mm in the DIC line profile.

CONCLUSIONS

An actuator-sensor PANI−optode tandem is demonstrated here for imaging CO_2 and DIC in environmental samples, including water, plants, and soils. 2D images and line profiles of the predominant inorganic carbon species are accessible before and after PANI-based acidification based on CO_2 optical readout. The analytical principle assumes that, when the sample is acidified to pH 4.5 or lower, all the carbonate species are converted to CO_2, thereby representing DIC. Before that, the optode provides pure CO_2 measurements according to its limit of detection. Importantly, in the case of solid samples (i.e., plants and soils), the images represent surface concentration profiles. To the best of our knowledge, this is the first time that spatial gradients of DIC are accessible in 2D with a resolution of <1 mm in environmental systems. The analytical operation of the developed PANI−optode concept was validated by comparing measurements of fresh and seawater samples to those obtained with conventional acid−base titrations. Moreover, the capability to provide CO_2 and DIC profiles in complex biogeochemical samples was proven with a leaf of the freshwater plant *V. spiralis* (dark respiration conditions) and in a $CaCO_3$-amended acidic waterlogged soil. The presented method is a powerful tool for the study of carbonate chemistry heterogeneities in any environmental system and may open new strategies for chemical imaging techniques of other pH-dependent analytes, such as total ammonia nitrogen or total dissolved sulfide, by simply changing the used sensor.

https://doi.org/10.1021/acssensors.3c00790
ACS Sens. 2023, 8, 2843−2851

■ ASSOCIATED CONTENT

Supporting Information

The Supporting Information is available free of charge at https://pubs.acs.org/doi/10.1021/acssensors.3c00790.

Experimental section, electropolymerization of polyaniline, electrochemical procedures, data analysis, calculations, details on soil composition, photos of setups, and complementary experiments (PDF)

■ AUTHOR INFORMATION

Corresponding Authors

Maria Cuartero − *Department of Chemistry, School of Engineering Science in Chemistry, Biochemistry and Health, KTH Royal Institute of Technology, Stockholm SE-100 44, Sweden; UCAM-SENS, Universidad Católica San Antonio de Murcia, UCAM HiTech, Murcia 30107, Spain;* orcid.org/0000-0002-3858-8466; Email: mariacb@kth.se

Klaus Koren − *Aarhus University Centre for Water Technology, Department of Biology, Section for Microbiology, Aarhus University, Aarhus 8000, Denmark;* orcid.org/0000-0002-7537-3114; Email: klaus.koren@bio.au.dk

Authors

Alexander Wiorek − *Department of Chemistry, School of Engineering Science in Chemistry, Biochemistry and Health, KTH Royal Institute of Technology, Stockholm SE-100 44, Sweden*

Fabian Steininger − *Aarhus University Centre for Water Technology, Department of Biology, Section for Microbiology, Aarhus University, Aarhus 8000, Denmark;* orcid.org/0000-0002-3326-6097

Gaston A. Crespo − *Department of Chemistry, School of Engineering Science in Chemistry, Biochemistry and Health, KTH Royal Institute of Technology, Stockholm SE-100 44, Sweden; UCAM-SENS, Universidad Católica San Antonio de Murcia, UCAM HiTech, Murcia 30107, Spain;* orcid.org/0000-0002-1221-3906

Complete contact information is available at: https://pubs.acs.org/10.1021/acssensors.3c00790

Author Contributions

A.W. and F.S. contributed equally to this work. All authors have given approval to the final version of the manuscript.

Notes

The authors declare no competing financial interest.

■ ACKNOWLEDGMENTS

This study was supported by research grants from the Swedish Research Council (VR-2019-04142, M.C.), the ÅForsk foundation (19-300, G.A.), and the Grundfos Foundation (K.K.). M.C. additionally acknowledges the funding from the European Research Council (ERC) under the European Union's Horizon 2020 research and innovation program (grant agreement no. 851957). We thank Lars B. Pedersen, Mette L. G. Nikolajsen, and Theresa Merl for technical support at Aarhus University.

■ REFERENCES

(1) Volk, T.; Hoffert, M. I. Ocean Carbon Pumps: Analysis of Relative Strengths and Efficiencies in Ocean-Driven Atmospheric CO_2 Changes. In *The Carbon Cycle and Atmospheric CO_2: Natural Variations Archean to Present*; Sundquist, E. T., Broecker, W. S., Eds.; American Geophysical Union, 2013; pp 99−110.

(2) Millero, F. J. The Marine Inorganic Carbon Cycle. *Chem. Rev.* **2007**, *107*, 308−341.

(3) Cole, J. J. Chapter 6—The Carbon Cycle: With a Brief Introduction to Global Biogeochemistry. In *Fundamentals of Ecosystem Science*; Weathers, K. C., Strayer, D. L., Likens, G. E., Eds.; Academic Press, 2013; pp 109−135.

(4) Hurd, C. L.; Beardall, J.; Comeau, S.; Cornwall, C. E.; Havenhand, J. N.; Munday, P. L.; Parker, L. M.; Raven, J. A.; McGraw, C. M. Ocean Acidification as a Multiple Driver: How Interactions between Changing Seawater Carbonate Parameters Affect Marine Life. *Mar. Freshwater Res.* **2020**, *71*, 263.

(5) Orr, J. C.; Fabry, V. J.; Aumont, O.; Bopp, L.; Doney, S. C.; Feely, R. A.; Gnanadesikan, A.; Gruber, N.; Ishida, A.; Joos, F.; Key, R. M.; Lindsay, K.; Maier-Reimer, E.; Matear, R.; Monfray, P.; Mouchet, A.; Najjar, R. G.; Plattner, G.-K.; Rodgers, K. B.; Sabine, C. L.; Sarmiento, J. L.; Schlitzer, R.; Slater, R. D.; Totterdell, I. J.; Weirig, M.-F.; Yamanaka, Y.; Yool, A. Anthropogenic Ocean Acidification over the Twenty-First Century and Its Impact on Calcifying Organisms. *Nature* **2005**, *437*, 681−686.

(6) Johnson, K. M.; King, A. E.; Sieburth, J. M. Coulometric TCO_2 Analyses for Marine Studies; an Introduction. *Mar. Chem.* **1985**, *16*, 61−82.

(7) O'Sullivan, D. W.; Millero, F. J. Continual Measurement of the Total Inorganic Carbon in Surface Seawater. *Mar. Chem.* **1998**, *60*, 75−83 Elsevier B.V..

(8) Dickson, A. G.; Sabine, C. L.; Christian, J. R. *Guide to Best Practices for Ocean CO2 Measurements*; PICES Special Publication, 2007; Vol. 3.

(9) Ahmerkamp, S.; Jalaluddin, F. M.; Cui, Y.; Brumley, D. R.; Pacherres, C. O.; Berg, J. S.; Stocker, R.; Kuypers, M. M. M.; Koren, K.; Behrendt, L. Simultaneous Visualization of Flow Fields and Oxygen Concentrations to Unravel Transport and Metabolic Processes in Biological Systems. *Cells Rep. Methods* **2022**, *2*, 100216.

(10) Koren, K.; Brodersen, K. E.; Jakobsen, S. L.; Kühl, M. Optical Sensor Nanoparticles in Artificial Sediments-a New Tool to Visualize O2 Dynamics around the Rhizome and Roots of Seagrasses. *Environ. Sci. Technol.* **2015**, *49*, 2286−2292.

(11) Honeyman, A. S.; Merl, T.; Spear, J. R.; Koren, K. Optode-Based Chemical Imaging of Laboratory Burned Soil Reveals Millimeter-Scale Heterogeneous Biogeochemical Responses. *Environ. Res.* **2023**, *224*, 115469.

(12) Athavale, R.; Pankratova, N.; Dinkel, C.; Bakker, E.; Wehrli, B.; Brand, A. Fast Potentiometric CO2 Sensor for High-Resolution in Situ Measurements in Fresh Water Systems. *Environ. Sci. Technol.* **2018**, *52*, 11259−11266.

(13) Brodersen, K. E.; Koren, K.; Revsbech, N. P.; Kühl, M. Strong Leaf Surface Basification and CO 2 Limitation of Seagrass Induced by Epiphytic Biofilm Microenvironments. *Plant, Cell Environ.* **2020**, *43*, 174−187.

(14) Roy, R. N.; Roy, L. N.; Vogel, K. M.; Porter-Moore, C.; Pearson, T.; Good, C. E.; Millero, F. J.; Campbell, D. M. The Dissociation Constants of Carbonic Acid in Seawater at Salinities 5 to 45 and Temperatures 0 to 45 °C. *Mar. Chem.* **1993**, *44*, 249−267.

(15) Steininger, F.; Revsbech, N. P.; Koren, K. Total Dissolved Inorganic Carbon Sensor Based on Amperometric CO 2 Microsensor and Local Acidification. *ACS Sens.* **2021**, *6*, 2529−2533.

(16) Steininger, F.; Zieger, S. E.; Koren, K. Dynamic Sensor Concept Combining Electrochemical PH Manipulation and Optical Sensing of Buffer Capacity. *Anal. Chem.* **2021**, *93*, 3822−3829.

(17) Afshar, M. G.; Crespo, G. A.; Bakker, E. Thin-Layer Chemical Modulations by a Combined Selective Proton Pump and PH Probe for Direct Alkalinity Detection. *Angew. Chem., Int. Ed.* **2015**, *54*, 8110.

(18) Wiorek, A.; Cuartero, M.; De Marco, R.; Crespo, G. A. Polyaniline Films as Electrochemical-Proton Pump for Acidification of Thin Layer Samples. *Anal. Chem.* **2019**, *91*, 14951−14959.

(19) Wiorek, A.; Hussain, G.; Molina-Osorio, A. F.; Cuartero, M.; Crespo, G. A. Reagentless Acid−Base Titration for Alkalinity Detection in Seawater. *Anal. Chem.* **2021**, *93*, 14130−14137.
(20) Chen, C.; Wiorek, A.; Gomis-Berenguer, A.; Crespo, G. A.; Cuartero, M. Portable All-in-One Electrochemical Actuator-Sensor System for the Detection of Dissolved Inorganic Phosphorus in Seawater. *Anal. Chem.* **2023**, *95*, 4180−4189.
(21) Steininger, F.; Wiorek, A.; Crespo, G. A.; Koren, K.; Cuartero, M. Imaging Sample Acidification Triggered by Electrochemically Activated Polyaniline. *Anal. Chem.* **2022**, *94*, 13647−13651.
(22) Zeebe, R. E.; Wolf-Gladrow, D. *CO_2 in Seawater: Equilibrium, Kinetics, Isotopes*; Halpem, D., Ed.; Elsevier Science, 2001; Vol. *65*.
(23) Zhu, K.; Bruun, S.; Larsen, M.; Glud, R. N.; Jensen, L. S. Heterogeneity of O2 Dynamics in Soil Amended with Animal Manure and Implications for Greenhouse Gas Emissions. *Soil Biol. Biochem.* **2015**, *84*, 96−106.
(24) Van Nguyen, Q.; Wu, D.; Kong, X.; Bol, R.; Petersen, S. O.; Jensen, L. S.; Liu, S.; Brüggemann, N.; Glud, R. N.; Larsen, M.; Bruun, S. Effects of Cattle Slurry and Nitrification Inhibitor Application on Spatial Soil O2 Dynamics and N2O Production Pathways. *Soil Biol. Biochem.* **2017**, *114*, 200−209.
(25) Clapham, W. M.; Zibilske, L. M. Wood Ash as a Liming Amendment. *Commun. Soil Sci. Plant Anal.* **1992**, *23*, 1209−1227.
(26) Molina-Osorio, A. F.; Wiorek, A.; Hussain, G.; Cuartero, M.; Crespo, G. A. Modelling Electrochemical Modulation of Ion Release in Thin-Layer Samples. *J. Electroanal. Chem.* **2021**, *903*, 115851.
(27) Jelle, B. P.; Hagen, G.; Hesjevik, S. M.; Ødegård, R. Reduction Factor for Polyaniline Films on Ito from Cyclic Voltammetry and Visible Absorption Spectra. *Electrochim. Acta* **1993**, *38*, 1643−1647.
(28) Michałowski, T.; Asuero, A. G. New Approaches in Modeling Carbonate Alkalinity and Total Alkalinity. *Crit. Rev. Anal. Chem.* **2012**, *42*, 220−244.
(29) Müller, J. D.; Schneider, B.; Rehder, G. Long-Term Alkalinity Trends in the Baltic Sea and Their Implications for CO 2 -Induced Acidification. *Limnol. Oceanogr.* **2016**, *61*, 1984−2002.
(30) Fischer, J. P.; Wenzhöfer, F. A Novel Planar Optode Setup for Concurrent Oxygen and Light Field Imaging: Application to a Benthic Phototrophic Community. *Limnol. Oceanogr.: Methods* **2010**, *8*, 254−268.
(31) Kühl, M.; Rickelt, L. F.; Thar, R. Combined Imaging of Bacteria and Oxygen in Biofilms. *Appl. Environ. Microbiol.* **2007**, *73*, 6289−6295.
(32) Dickson, A. G.; Riley, J. P. The Effect of Analytical Error on the Evaluation of the Components of the Aquatic Carbon-Dioxide System. *Mar. Chem.* **1978**, *6*, 77−85.
(33) Sumner, M. E.; Noble, A. D. Soil Acidification: The World Story. In *Handbook of Soil Acidity*; Rengel, Z., Ed.; CRC Press: New York, NY, 2003; pp 1−28.
(34) Haling, R. E.; Simpson, R. J.; Culvenor, R. A.; Lambers, H.; Richardson, A. E. Effect of Soil Acidity, Soil Strength and Macropores on Root Growth and Morphology of Perennial Grass Species Differing in Acid-Soil Resistance. *Plant, Cell Environ.* **2011**, *34*, 444−456.
(35) Ma, J. F. Syndrome of Aluminum Toxicity and Diversity of Aluminum Resistance in Higher Plants. *Int. Rev. Cytol.* **2007**, *264*, 225−252.
(36) Haling, R. E.; Simpson, R. J.; Delhaize, E.; Hocking, P. J.; Richardson, A. E. Effect of Lime on Root Growth, Morphology and the Rhizosheath of Cereal Seedlings Growing in an Acid Soil. *Plant Soil* **2010**, *327*, 199−212.

https://doi.org/10.1021/acssensors.3c00790
ACS Sens. 2023, 8, 2843−2851